ACS central science

Research Article

http://pubs.acs.org/journal/acscii

Direct in Situ Measurement of Charge Transfer Processes During Photoelectrochemical Water Oxidation on Catalyzed Hematite

Jingjing Qiu,[†] Hamed Hajibabaei,[‡] Michael R. Nellist,[†] Forrest A. L. Laskowski,[†] Thomas W. Hamann,[‡] and Shannon W. Boettcher*[,†]

[†]Department of Chemistry and Biochemistry, Materials Science Institute, University of Oregon, Eugene, Oregon 97403, United States
[‡]Department of Chemistry, Michigan State University, East Lansing, Michigan 48824, United States

Supporting Information

ABSTRACT: Electrocatalysts improve the efficiency of light-absorbing semiconductor photoanodes driving the oxygen evolution reaction, but the precise function(s) of the electrocatalysts remains unclear. We directly measure, for the first time, the interface carrier transport properties of a prototypical visible-light-absorbing semiconductor, α-Fe_2O_3, in contact with one of the fastest known water oxidation catalysts, $Ni_{0.8}Fe_{0.2}O_x$, by directly measuring/controlling the current and/or voltage at the $Ni_{0.8}Fe_{0.2}O_x$ catalyst layer using a second working electrode. The measurements demonstrate that the majority of photogenerated holes in α-Fe_2O_3 directly transfer to the catalyst film over a wide range of conditions and that the $Ni_{0.8}Fe_{0.2}O_x$ is oxidized by photoholes to an operating potential sufficient to drive water oxidation at rates that match the photocurrent generated by the α-Fe_2O_3. The $Ni_{0.8}Fe_{0.2}O_x$ therefore acts as both a hole-collecting contact and a catalyst for the photoelectrochemical water oxidation process. Separate measurements show that the illuminated junction photovoltage across the α-Fe_2O_3|$Ni_{0.8}Fe_{0.2}O_x$ interface is significantly decreased by the oxidation of Ni^{2+} to Ni^{3+} and the associated increase in the $Ni_{0.8}Fe_{0.2}O_x$ electrical conductivity. In sum, the results illustrate the underlying operative charge-transfer and photovoltage generation mechanisms of catalyzed photoelectrodes, thus guiding their continued improvement.

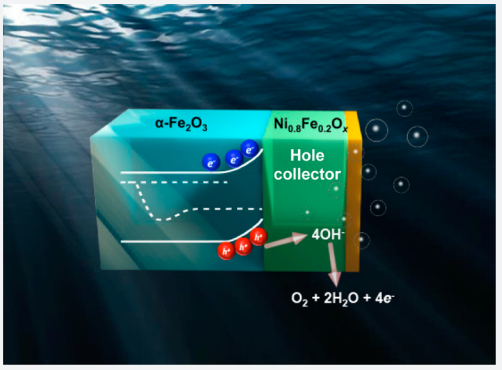

INTRODUCTION

Solar-driven water splitting is a possible route to scalable solar-to-fuel conversion.[1−3] Water splitting consists of a cathodic hydrogen evolution reaction (HER) and an anodic oxygen evolution reaction (OER). In particular, the OER (e.g., $4OH^- \rightarrow 2H_2O + O_2 + 4e^-$ in basic media) is inefficient, owing in part to the high kinetic overpotential associated with the reaction.[4]

Semiconductor (sem) photoanodes are typically decorated with electrocatalysts (cat) to minimize OER overpotential losses. OER catalysts such as IrO_x,[5,6] Co-Pi,[7,8] and Ni(Fe)-OOH[9−12] lower the photocurrent onset potential of semiconductor photoanodes including $BiVO_4$,[12] α-Fe_2O_3,[5,6,10,13] and n-Si.[11] Electrolyte-permeable electrocatalysts, which are porous at a molecular level, like Co-Pi and Ni(Fe)OOH, appear particularly well-suited for direct interfacing with oxide photoanodes. For example, the performance of the visible-light-absorbing photoanode α-Fe_2O_3 improves with either Co-Pi[8] or "amorphous" $NiFeO_x$ integration.[9] Kim et al. compared two types of electrocatalysts on nanoporous $BiVO_4$, FeOOH, and NiOOH, and showed that the combination of these electrolyte-permeable catalysts yielded optimal performance compared to a single electrocatalyst component.[12] Multiple techniques, including transient absorption spectroscopy (TAS)[14−16] and photoelectrochemical impedance spectroscopy (PEIS),[5,7] have been employed to elucidate the mechanisms underlying this performance enhancement. However, the role of electrocatalysts on semiconductor photoanodes remains an area of active study with many different hypotheses proposed. The underlying challenge is that there are a number of competing electron and hole transfer pathways from the semiconductor to the catalyst and/or solution that are difficult to distinguish between using conventional measurements. Improved understanding of the various roles of the electrocatalyst layer will allow the design of higher efficiency photoelectrode systems.

Barroso et al. tracked the lifetime of holes in hematite by TAS and observed similar spectra for α-Fe_2O_3|Co-Pi without anodic bias and bare α-Fe_2O_3 with anodic bias.[15] Because anodic biasing of α-Fe_2O_3 depletes the surface electron density and hinders electron−hole pair recombination, they proposed that CoO_x (i.e., the cobalt (oxy)hydroxide layer resulting from Co-Pi electrodeposition or other similar Co-based treatments) plays a similar role to the anodic bias by forming a Schottky-type heterojunction that increases the band bending in the α-Fe_2O_3.[15] They further observed that the electron and hole recombination in α-Fe_2O_3 is biphasic; the slow decay phase was assigned to "long-lived holes".[14] TAS further revealed that both

Received: July 12, 2017
Published: August 17, 2017

DOI: 10.1021/acscentsci.7b00310
ACS Cent. Sci. 2017, 3, 1015−1025

α-Fe_2O_3|Ga_2O_3 and α-Fe_2O_3|CoO_x electrodes require less anodic bias than the bare α-Fe_2O_3 counterparts to form "long-lived holes".[14] This led to the hypothesis that CoO_x enhances the spatial extent of the electron depletion layer instead of collecting holes, and that water oxidation directly occurs at the surface of α-Fe_2O_3.[14,15] Wang and co-workers applied intensity modulated photocurrent spectroscopy (IMPS) to study the kinetics of hole transfer and electron/hole recombination in the α-Fe_2O_3 and α-Fe_2O_3|$NiFeO_x$ systems.[17] They found that the apparent rate of recombination decreases more than that of hole transfer in the α-Fe_2O_3|$NiFeO_x$ photoelectrode, compared to an uncatalyzed control sample, and proposed that $NiFeO_x$ primarily serves as a passivation layer rather than a catalytic layer.[17] It is unclear, however, the extent to which the relative simple models used to analyze the IMPS data[18] apply to complicated catalyzed photoelectrodes that have both surface states and heterogeneous catalyst layers that probably generate a distribution of electronic states.[11,19] Further, the concentration of Fe in NiOOH can change its properties, such as electrical conductivity, stability, and OER activity.[20−22] It has been proposed that Fe contents in excess of 20% can lead to the formation of separate, Fe-rich phases in Ni(Fe)OOH,[23] which could increase the heterogeneity of the electrocatalyst and lower electrical conductivity.

In contrast to the above studies, Gamelin and co-workers proposed that the photogenerated holes in mesoporous α-Fe_2O_3 are converted to oxidizing equivalents in Co-Pi that produce O_2.[13] However, they also observed that the photocurrent decreased in mesoporous α-Fe_2O_3 with increasing Co-Pi thickness, which they attribute to interface recombination between photogenerated conduction-band electrons and accumulated holes in Co-Pi, which is referred to as a "kinetic bottleneck".[13,24] The film-thickness-dependence of Co-Pi on α-Fe_2O_3 was also investigated on planar α-Fe_2O_3 films prepared with atomic layer deposition (ALD) by Hamann and co-workers, using photoelectrochemical and impedance measurements.[7] The found that thicker catalyst layers perform better and proposed that the Co-Pi catalyst collects and stores photogenerated holes from the hematite electrode and thicker Co-Pi films increase charge separation and surface area of the porous catalytic film.[7] The difference between the two studies might result from (1) parasitic optical absorbance in the catalyst layer[25] when it is deposited on the mesoporous sample compared to the planar sample (where backside illumination of a planar structure can be used effectively to avoid light absorption in the catalyst), or (2) the increased possibility of direct charge transfer between the underlying conducting oxide and catalyst layer for thicker catalyst layers used in the mesoporous system.

Similar to Co-based electrocatalysts, Young and Hamann also showed that electrolyte-permeable nickel (oxy)hydroxide collects holes from α-Fe_2O_3 by current transient measurements; the NiOOH modified photoelectrodes were shown to accumulate 100-fold more "surface" charge than bare α-Fe_2O_3, consistent with holes accumulating in the catalyst layer.[10]

These above examples, and the associated differing proposed mechanisms, demonstrate the need for quantitative and direct measurements to distinguish between the effects of surface treatments on recombination ("passivation"), changes to interfacial electronics, and on charge carrier transfer (catalysis).[4]

One approach to quantitatively understand the semlcat interface is to directly probe/control the electrocatalyst potential relative to that of the semiconductor in photoelectrochemical (PEC) water oxidation. We developed a dual-working-electrode (DWE) strategy for in situ measurement of the electrocatalyst potential under applied bias of the semiconductor in the dark and light, and applied it to model single-crystalline TiO_2 photoelectrodes.[19,26] We found that electrolyte-permeable electrocatalysts, such as Ni(Fe)OOH, form a so-called "adaptive" junction with TiO_2, while dense electrocatalysts, such as IrO_x, form a buried junction with TiO_2.[26] The adaptive junctions formed via the electrolyte-permeable electrocatalyst produced an increased open-circuit voltage (V_{oc}) at the interface due to electrocatalyst oxidation during OER (thereby increasing the "effective" electronic barrier height).[26] The key feature of electrocatalysts that form such adaptive junctions appears to be the ability of electronic charge (i.e., holes) to be stored on the electrocatalyst layer but remain electrostatically screened by mobile electrolyte ions in the catalyst layer.[11,19] In an ideal adaptive interface this would increase the catalyst's electrochemical potential without affecting band alignment of the semiconductor with the solution. This effect thus can be thought of as a way to produce a "more-favorable" energy level alignment between catalyst and semiconductor that can increase the photovoltage relative to unoptimized buried semlcat junctions where the interfacial energetics are fixed by the solid interface.[11,19,26,27]

The insights obtained from the studies on the single-crystalline TiO_2 model system[26] suggest that the semlcat junction type is important in determining photoanode performance. However, because TiO_2 has a deep (i.e., highly oxidizing) valence band, it is not clear that the results will apply to all photoanodes, especially to visible-light-absorbing polycrystalline oxides. For instance, α-Fe_2O_3 has a much less oxidizing valence-band-edge position and higher density of surface states compared to TiO_2.[28−30] To design efficient polycrystalline visible-light-absorbing oxide photoanodes, it is therefore useful to identify the junction behavior and elucidate the semlcat interface charge-transfer processes in materials such as α-Fe_2O_3.

Here we report a mechanistic study of the α-Fe_2O_3|$Ni_{0.8}Fe_{0.2}O_x$ interfacial properties using DWE photoelectrochemistry experiments—for the first time applied to visible-light-absorbing oxide photoanodes. Conformal and crack-free films of α-Fe_2O_3 and $Ni_{0.8}Fe_{0.2}O_x$ were prepared with ALD[31] and photochemical metal−organic deposition (PMOD),[32] respectively, to make robust (nonshorting) DWE catalyzed photoelectrode devices ideally suited for such fundamental study. The electrical and catalytic properties of $Ni_{0.8}Fe_{0.2}O_x$ electrocatalyst films were analyzed in parallel on indium tin oxide (ITO) substrates using similar DWE architectures. We demonstrate that the electrical conductivity of the $Ni_{0.8}Fe_{0.2}O_x$ electrocatalyst prepared via PMOD is potential-dependent, and the α-Fe_2O_3|$Ni_{0.8}Fe_{0.2}O_x$ interfacial properties change with the oxidation state of the electrocatalyst layer. Importantly, we show that a fully activated $Ni_{0.8}Fe_{0.2}O_x$ electrocatalyst layer can harvest up to 95% of the photogenerated holes in α-Fe_2O_3 at steady state under relevant water oxidation conditions. These results quantitatively demonstrate the role of the catalyst layer as a hole collector.

DOI: 10.1021/acscentsci.7b00310
ACS Cent. Sci. 2017, 3, 1015−1025

RESULTS AND DISCUSSION

Intrinsic Properties of $Ni_{0.8}Fe_{0.2}O_x$ Catalyst Films. The deposition of a conformal and crack-free electrocatalyst film is critical in making DWE devices without shorts between the top porous Au electrode and the semiconducting or conducting oxide substrate. The amorphous Ni−Fe oxide electrocatalyst film deposited via PMOD is suitable for this purpose and possesses respectable OER performance.[22,32] Smith et al. investigated a series of amorphous Ni−Fe oxide films with different Ni/Fe ratios.[22] They found that the $Ni_{0.8}Fe_{0.2}O_x$ film composition produces optimal catalytic properties,[22] consistent with related studies on the Ni−Fe oxyhydroxide catalysts.[21] Clean and residue-free substrate surfaces are critical to spin-coating crack-free films; the cleaning procedure as described in the experimental section (Supporting Information) achieves this goal. In addition, the annealing time is important. We used Fourier transform infrared (FTIR) spectroscopy to track the ligand residue[32] and found that 70 min of UV-annealing yielded $Ni_{0.8}Fe_{0.2}O_x$ films with little ligand residue (Figure S1) and produced a smooth, uniform film on the ITO substrate (Figure 1a). The root-mean-squared surface roughness of the deposited film on a 9-μm^2 area was ∼1 nm by atomic force microscopy (AFM) (Figure S2). This smoothness allows for the deposition of a thin layer of the interconnected Au film forming WE2. The electrocatalyst film on an ITO substrate exhibits an anodic peak at ∼0.25 V vs ε_{O_2/OH^-} in the cyclic voltammogram (CV), typical for the nominally $Ni^{2+/3+}$ redox process in Ni(Fe)OOH (Figure 1b),[32,33] and the OER current is similar to Ni(Fe)OOH prepared with different approaches.[21,34] The reduction waves grow with CV cycles and shift cathodically, indicating the activation of the film to the electrolyte-permeable Ni(Fe)OOH phase (Figure S3c). More than 70% of Ni sites in a 65 nm-thick film are activated within 15 CV scans (scan rate = 10 mV·s^{-1}), as determined by comparison of the redox wave integration to the known Ni quantity in the deposited film (measured by QCM mass measurement, see Figure S3).

When interfaced with the semiconductor, electrocatalysts must be sufficiently conductive to support charge transport through the catalyst film with a negligible potential drop. In scenarios where the catalyst is not sufficiently conductive, a portion of the applied potential will drop across the catalyst film to drive the current transport, or, for sufficiently high resistances, the kinetics of OER directly on or near the hematite surface may outcompete hole transfer and catalysis through the bulk catalyst film. The electrical conductivity of the electrocatalyst is also important for meaningful DWE measurements; the charge carriers must travel through the thickness of the catalyst layer to WE2, the Au top layer, to be measured. It is known that NiOOH is electrically conductive while $Ni(OH)_2$ is an insulator.[21,26,35]

Although $Ni_{0.8}Fe_{0.2}O_x$ has been shown to be an effective electrocatalyst,[22] little is known about its electrical conductivity under applied biases and thus what fraction of the film is responsible for catalysis. We therefore applied the ITO|$Ni_{0.8}Fe_{0.2}O_x$|Au DWE architecture to measure the through-film conductivity in situ as a function of potential. The film is conditioned through a series of CV cycles from WE2 (scan rate = 50 mV·s^{-1}, cycle numbers ranging from 30 to 50 until the redox peak does not change) to activate the electrocatalyst film. After activation, the integrated charge in the Ni(Fe)OOH reduction wave in CVs collected from either WE is identical (Figure S4b), indicating that the number of active Ni sites

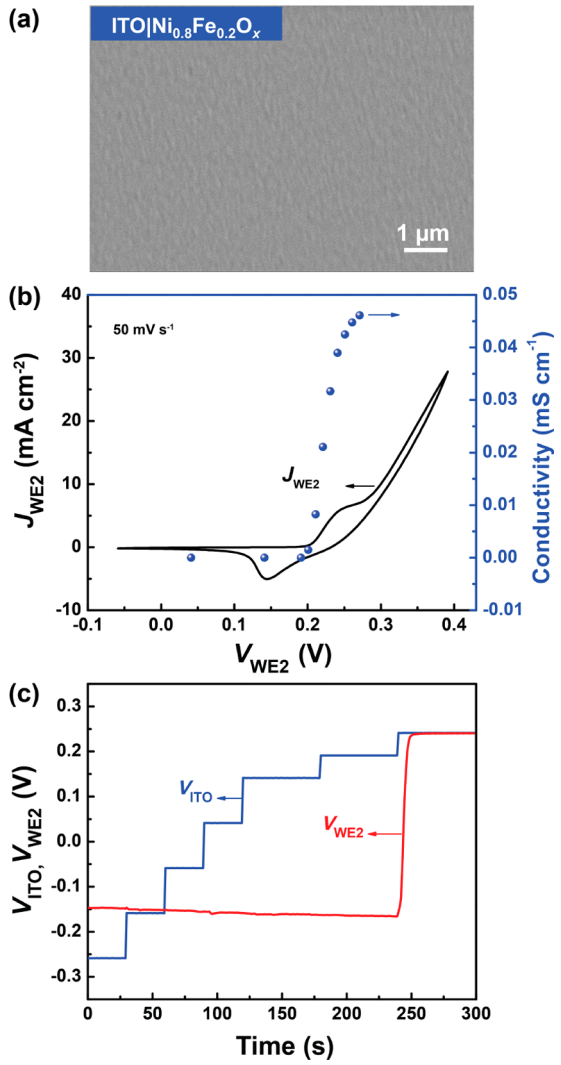

Figure 1. Catalytic and electrical properties of $Ni_{0.8}Fe_{0.2}O_x$. (a) SEM image of a conformal and crack-free $Ni_{0.8}Fe_{0.2}O_x$ film on an ITO substrate. (b) CV scan and in situ measurement of conductivity (at steady-state, held at each point for 3 min) of $Ni_{0.8}Fe_{0.2}O_x$ film on ITO. (c) In situ recording of V_{WE2} versus V_{ITO} (controlled by WE1 in chronoamperometry steps). The drift of V_{WE2} when the electrocatalyst is insulating is due likely to the slow equilibration between the Au layer and poorly defined solution/catalyst-film species. The voltages V_{WE2} and V_{ITO} are both reported relative to the thermodynamic redox potential for the OER.

accessed by the ITO and Au layer are equivalent (∼6.3 mC·cm^{-2} for this device) and the electrocatalyst film is sufficiently electrolyte-permeable.

Steady-state in situ film conductivity measurements were then performed by holding the potentials of both WEs at the same value for 10 s followed by stepping the potential of WE1 anodic by 5 mV (Figure S4c). The measured current was allowed to stabilize for 3 min before collecting each data point. The current change measured at WE2 is approximately the through-film-conduction current (as the potential of WE2 is kept constant during the measurement and hence any changes to the net current flowing are largely due to electronic conduction to WE2 from WE1):

$$\Delta I_{WE2} = I_{cond} \quad (1)$$

The effective catalyst film conductivities σ are estimated by

DOI: 10.1021/acscentsci.7b00310
ACS Cent. Sci. 2017, 3, 1015−1025

$$\sigma = \frac{I_{cond} \cdot d}{\Delta V \cdot A} \quad (2)$$

where d is the film thickness (here 100 nm), A is the geometric surface area of the electrode, and ΔV is the voltage offset between WE1 and WE2 (here 5 mV).

The measured current changes of both WEs are shown in Figure S4d. The conductivities of $Ni_{0.8}Fe_{0.2}O_x$ film are then derived from ΔI_{WE2} versus the applied potentials, as shown in Figure 1b. While the reduced film exhibits negligible conductivity, a sharp increase in conductivity is observed upon Ni oxidation. The oxidized Ni(Fe)OOH film with 20% Fe shown here has $\sigma \approx 0.05$ mS·cm^{-1} after 50 CV cycles. The range in the measured σ of different devices is less than 1 order of magnitude.

The transition in electrical conductivity of the Ni(Fe)OOH film is also reflected in the in situ sensing of V_{WE2}. The potential of ITO (WE1) was stepped and held at a constant value for 30−60 s, and the potential at the top of the $Ni_{0.8}Fe_{0.2}O_x$ film was recorded via the Au layer (WE2). V_{WE2} does not follow the potential change of WE1 until the catalyst film is oxidized and becomes conductive, i.e., when V_{ITO} reaches ∼0.23 V vs ε_{O_2/OH^-} or higher (Figure 1c). The sharp transition of V_{WE2} is consistent with the conductivity change trend (Figure 1b).

Understanding the electrocatalyst film's electrical conductivity transition is important because it determines the efficiency of charge transport through the film after hole collection from the semiconductor and before water oxidation. A conductive electrocatalyst network will facilitate the relay of photogenerated holes with a negligible potential drop as well as reduce the accumulation of holes at the semlcat interface. It also ensures that the DWE measurement via the Au layer accurately measures the interface energetics.

Interfacial Properties of $Ni_{0.8}Fe_{0.2}O_x$ on Hematite. *J−V Response of Photoelectrodes.* Deposition of the $Ni_{0.8}Fe_{0.2}O_x$ film onto a α-Fe_2O_3 photoanode reduces the root-mean-squared surface roughness from 21 to 3 nm (Figure 2). Additionally, the onset potential of α-Fe_2O_3|$Ni_{0.8}Fe_{0.2}O_x$ under one-sun illumination cathodically shifts by more than 100 mV (Figure 2c). The photocurrent of the $Ni_{0.8}Fe_{0.2}O_x$ functionalized α-Fe_2O_3 photoelectrode also improves, especially in the low-applied-bias regime (Figure 2c), in agreement with previous reports.[9,10] A thin electrolyte-permeable Au film was deposited on the α-Fe_2O_3|$Ni_{0.8}Fe_{0.2}O_x$ substrate to form the α-Fe_2O_3|$Ni_{0.8}Fe_{0.2}O_x$|Au DWE device (Figure S5). Because of backside illumination (i.e., from the FTO side of the hematite electrode), the photoexcitation density in the α-Fe_2O_3 in the DWE configuration is similar to that of non-DWE devices without the Au top layer (Figure S5d). CVs of the $Ni_{0.8}Fe_{0.2}O_x$ film collected via the Au top contact are also similar to those on ITO (Figure S4). This indicates that the Au film is sufficiently porous, allowing for free movement of ions and resulting in a negligible contribution to the current. Conditioning of the $Ni_{0.8}Fe_{0.2}O_x$ film was performed through CV scans of the electrocatalyst layer from WE2 in the dark and WE1 under light illumination, after Au deposition, until the integrated charge in the Ni reduction peak remained constant. While conditioning through WE2 is, of course, not possible on conventional photoelectrodes with only an ohmic back contact to the semiconductor,[36] it was used here for simplicity and the ability to directly monitor the size of the Ni redox wave during the conditioning process. The resulting (oxy)hydroxide phases are expected to be similar to those that would form on conventional photoelectrodes under OER conditions, although the time scales for conversion are likely different.

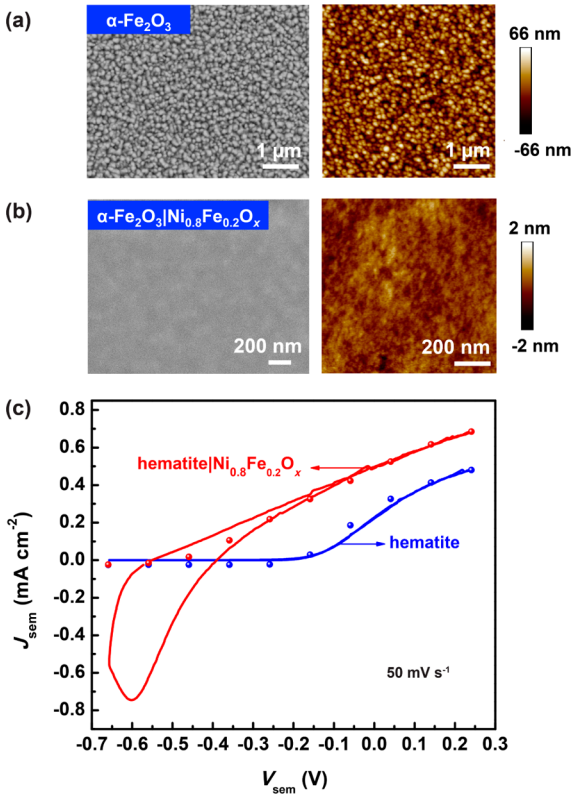

Figure 2. Morphological and photoelectrochemical properties of α-Fe_2O_3 and α-Fe_2O_3|$Ni_{0.8}Fe_{0.2}O_x$ photoelectrodes. Surface morphologies of (a) bare α-Fe_2O_3 and (b) α-Fe_2O_3|$Ni_{0.8}Fe_{0.2}O_x$ assessed by SEM and AFM imaging. (c) $J-V$ characterization of bare α-Fe_2O_3 and α-Fe_2O_3|$Ni_{0.8}Fe_{0.2}O_x$ photoelectrodes under one-sun backside illumination. The symbols show the steady-state photocurrent densities for the two electrodes. The voltage $V_{sem} = V_{WE1}$ is reported relative to the thermodynamic redox potential for the OER.

In Situ Measurement of the Catalyst Potential. Direct measurement of V_{cat} under fuel-producing conditions on α-Fe_2O_3 was performed through WE2 after activation of the electrocatalyst film. Representative postconditioned CV scans from both WEs are shown in Figure 3a. The steady-state potential of the electrocatalyst layer was recorded while controlling the potential of the α-Fe_2O_3 electrode. On the basis of the previous in situ measurement of the conductivity of $Ni_{0.8}Fe_{0.2}O_x$, the electrocatalyst layer should become conductive after being oxidized sufficiently to form nominally Ni(Fe)-OOH. The potential to initiate this electrical conductivity transition is ∼0.23 V vs ε_{O_2/OH^-} when measured on a conductive substrate, according to the in situ measurement performed on the ITO|$Ni_{0.8}Fe_{0.2}O_x$|Au DWE (Figure 1b). In the dark, the electrocatalyst layer can only be oxidized through leakage current from the n-type α-Fe_2O_3, which is under reverse bias at anodic potentials. Such dark leakage current across the α-Fe_2O_3|$Ni_{0.8}Fe_{0.2}O_x$ junction remains negligible up to V_{sem} = 0.24 V vs ε_{O_2/OH^-} (Figure S6a). It thus takes hours to charge the $Ni_{0.8}Fe_{0.2}O_x$ film in the dark and V_{WE2} (V_{cat}) responds very slowly to changes in V_{sem} (Figure S6b). Under illumination, however, a rapid transition of V_{WE2} (V_{cat}) occurs when V_{sem} = −0.45 V vs ε_{O_2/OH^-} (Figure 3b,c). The decrease in applied voltage (∼0.7 V) required to initiate the conductivity switch

DOI: 10.1021/acscentsci.7b00310
ACS Cent. Sci. 2017, 3, 1015−1025

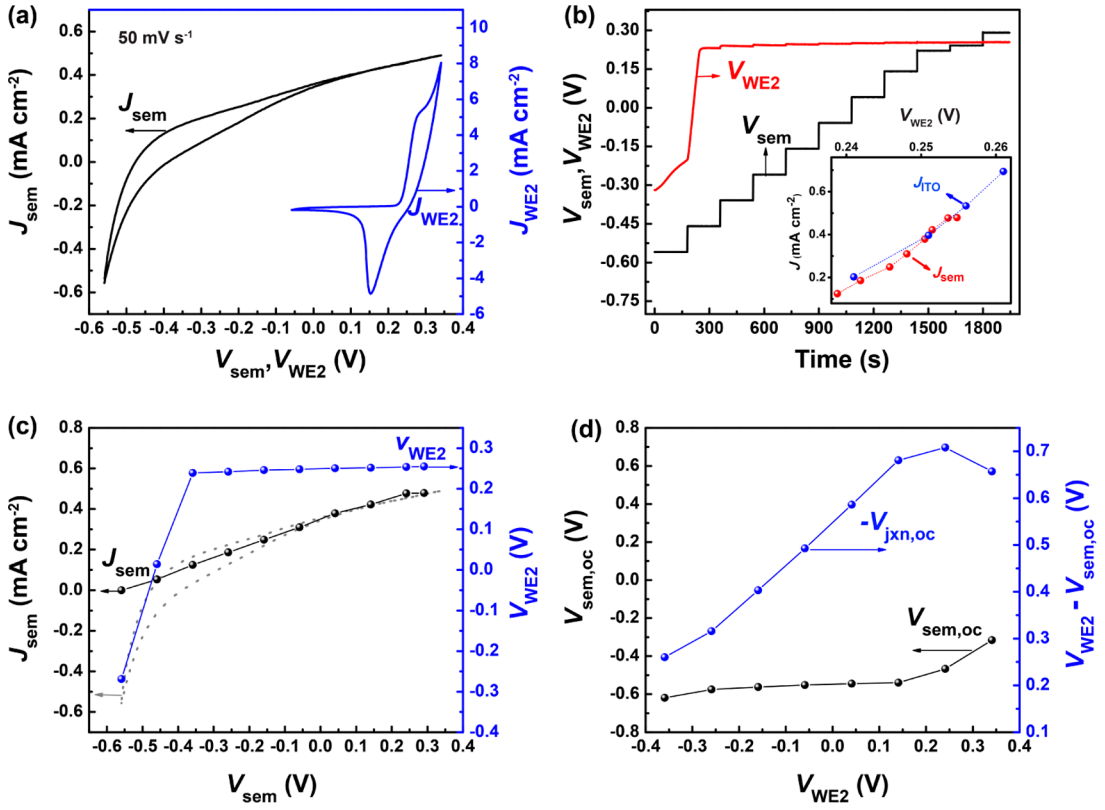

Figure 3. Interfacial DWE photoelectrochemical characterization of α-Fe_2O_3|$Ni_{0.8}Fe_{0.2}O_x$|Au. (a) Illuminated CVs, collected separately, for a representative DWE device under illumination measured through WE1 (controlling V_{sem}) and WE2 (controlling V_{WE2}). (b) Illuminated in situ measurements of V_{cat} in response to V_{sem} chronoamperometry steps. The inset shows the current densities of ITO (J_{ITO}, blue dots) and illuminated hematite (J_{sem}, red dots) that lead to the measured potentials at WE2 (V_{WE2}) on the catalyst surface. The fact that V_{WE2} are the same in both cases is strong evidence the $Ni_{0.8}Fe_{0.2}O_x$ layer is catalyzing the photoelectrochemical OER on the hematite surface, as it is on the ITO electrode. (c) Superimposed V_{WE2} (V_{cat}) response on the steady-state current density of the illuminated semiconductor. The dashed curve is the CV of the illuminated semiconductor. (d) The $V_{sem,oc}$ of α-Fe_2O_3 and the $V_{jxn,oc}$ for α-Fe_2O_3|$Ni_{0.8}Fe_{0.2}O_x$ both as a function of V_{WE2} (V_{cat}) under illumination. The voltages V_{sem} and V_{WE2} are relative to the thermodynamic redox potential for the OER in all panels.

under illumination is attributed to the generation of photoholes and subsequent photovoltage build-up across the semlcat interface.

The generation of minority holes in hematite under light illumination causes the hole quasi-Fermi level ($E_{f,p}$) to move down (i.e., more oxidizing) from $E_{f,n}$ (Scheme 1). Both electrons and holes may transfer to the catalyst layer. The magnitude of the (majority carrier) electron flow is in large part determined by the built-in potential (i.e., degree of band-bending) at the semlcat interface, and the density of electron acceptor states in the catalyst layer. The net transfer of holes is driven by the energy difference between the hole quasi-Fermi level ($E_{f,p}$) and the Fermi level of the catalyst (E_{cat}). We note that in Scheme 1 the general shape of the hole quasi Fermi level is adapted from related simulations.[27] If holes are flowing at steady state there must be a gradient in $E_{f,p}$, as depicted moving toward the surface of the semiconductor.

Scheme 1. Schematic Band Diagram of an Illuminated α-Fe_2O_3|$Ni_{0.8}Fe_{0.2}O_x$|Au Device

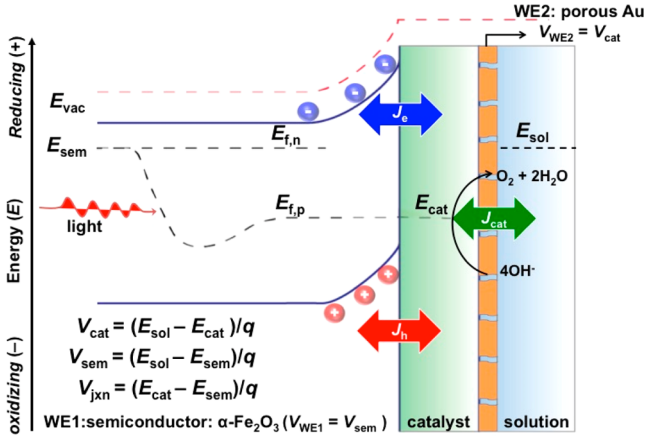

From the current–voltage response in Figure 3a, we see that the net current ($J_{sem} = J_e + J_h$) is positive for $V_{sem} > -0.45$ V vs ε_{O_2/OH^-} under illumination. At steady state this net positive current can either drive water oxidation on the semiconductor surface (as the catalyst is permeable to electrolyte), or the holes can accumulate in the catalyst layer, charge it, and then drive OER current from the catalyst. Figure 3c shows that V_{WE2} (V_{cat}) increases rapidly to 0.25 V vs ε_{O_2/OH^-} as soon as $V_{sem} > -0.45$ V vs ε_{O_2/OH^-} under illumination. This demonstrates the catalyst charges with photoexcited minority holes from the semiconductor layer. The abrupt transition of V_{WE2} (V_{cat}) relative to V_{sem} is consistent with that of the TiO_2|Ni(Fe)OOH interface studied with DWE photoelectrochemistry previously.[26]

Further anodic biasing of hematite by raising V_{sem} increases the electron depletion width in the semiconductor, and thus increases the photocurrent density, J_{sem}, by improving bulk

DOI: 10.1021/acscentsci.7b00310
ACS Cent. Sci. 2017, 3, 1015–1025

carrier collection and decreasing surface recombination from electronic currents (Figure 3a).[37] As V_{sem} is increased we observe small incremental increases in V_{WE2} (V_{cat}) (Figure S7). This is consistent with an increased oxidation of the electrocatalyst layer (equivalent to shifting the Fermi level of the electrocatalyst down in Scheme 1) by a higher hole flux and a decrease in the electron transfer rate. Both processes will affect the steady-state net hole concentration on the electrocatalyst and thus V_{WE2} (V_{cat}), and subsequently lead to an increased rate of water oxidation on the catalyst layer at steady state to maintain current continuity with the semiconductor. These data suggest that the electrocatalyst layer is effectively collecting holes from the semiconductor and accumulating them until a sufficiently high potential is reached such that water oxidation can occur. The efficiency of this hole transfer process is discussed further below.

Interface Photovoltage Measurements. Because the Ni(Fe)OOH electrocatalyst is electrolyte-permeable, the injected charges in principle can shift E_{cat} relative to the semiconductor band edges as charge neutrality (i.e., screening of the injected holes) can be achieved via electrolyte ion flow in/out of the electrocatalyst (we termed this previously an "adaptive" junction).[10,21,26] In traditional PEC analysis, the open-circuit potential of a semiconductor photoelectrode is measured under illumination as the potential of the back contact to the semiconductor relative to the solution potential (here ε_{O_2/OH^-}) without the knowledge of the potential of the catalyst. Independent control and sensing of V_{WE2} (V_{cat}) allow us to probe the junction photovoltage across the semiconductor and electrocatalyst directly, where the quasi-equilibrium is established between the semiconductor and the catalyst under illumination. To do this we use WE1 to measure V_{sem} at open circuit ($V_{sem,oc}$) as a function of V_{WE2}. We find that the dependence of $V_{sem,oc}$ on V_{WE2} (V_{cat}) is affected by the conductivity of the electrocatalyst layer (Figure 3d). When the electrocatalyst layer is insulating (V_{cat} < 0.23 V vs ε_{O_2/OH^-}), $V_{sem,oc}$ is constant and thus the semlcat junction photovoltage ($V_{jxn,oc}$) increases with V_{WE2} (V_{cat}). This results from the fact that the electrically insulating, but electrolyte-permeable, catalyst layer leaves the semiconductor unaffected by changing V_{WE2} (V_{cat}). When the catalyst layer becomes conductive (V_{WE2} > 0.23 V vs ε_{O_2/OH^-}), $V_{jxn,oc}$ decreases in magnitude. This observation is inconsistent with the simple "adaptive" junction picture, where an increase in the catalyst voltage should lead to a concomitant increase in the junction photovoltage until a limit, set by the semiconductor recombination and carrier transport, is reached.[27] Experimentally, the same decrease in $V_{jxn,oc}$ with the oxidation of Ni(Fe) catalyst is not observed in single-crystalline TiO_2 photoanodes.[26] The simple adaptive-junction model requires that the catalyst electronic properties—particularly the effective density of states able to collect holes and electrons from the valence and conduction bands, respectively—must be unaffected by the potential applied to the catalyst. This criterion may not hold in this situation.

Under open-circuit conditions, the net current flow in the semiconductor is zero; therefore, the electron current (J_e) is constant and is equal to the hole current (J_h). One simple model for electron transfer (the majority charge carrier) from the semiconductor to the catalyst is the quasi-first-order kinetic process[38] where the electron current is given by

$$J_e(V) = -q \cdot k_{et} \cdot [A] \cdot n_s \quad (3)$$

in which J_e is the current density ($A \cdot cm^{-2}$), k_{et} is the electron transfer rate constant ($cm^4 \cdot s^{-1}$), n_s is the density of electrons (cm^{-3}) at the hematite surface (set by the band bending and majority carrier bulk concentration), and [A] is the concentration of electron acceptor sites (cm^{-3}) capable of being reduced. Although the band structure is undoubtedly more complex, the electron acceptor, A, could be considered a Ni^{3+} site which can be reduced to nominally Ni^{2+} (ultimately forming $Ni(OH)_2$ which is then not able to be further easily reduced). One explanation, therefore, for the decrease in the junction photovoltage at V_{WE2} > 0.23 V vs ε_{O_2/OH^-} is that as [Ni^{3+}] increases, n_s must concomitantly decrease such that the electron and hole currents are kept equal. The primary mechanism to decrease n_s is through an increase in the depletion width (i.e., band-bending) by the movement of $V_{sem,oc}$ more positive, hence reducing the semlcat junction photovoltage. In other words, the electronic current flowing from the surface of hematite to the catalyst increases as V_{cat} moves to more positive potentials. This analysis is thus consistent with the view that it is the balance of electron and hole transfer to the catalyst that determines the semlcat junction photovoltage.

Other similar mechanisms involving surface states could also affect the interface photovoltage.[39] When the catalyst is held at a potential where the catalyst film is predominantly Ni^{2+}, charge that would otherwise accumulate in the surface states (and likewise lead to an increased electronic, i.e. recombination, current) can instead be transferred to the catalyst layer. Once the catalyst is oxidized to a higher level, the surface state can also accumulate more positive charge (as the surface-states and catalyst, being in direct contact, should be in quasi-equilibrium). This process would also lead to increased electronic current (i.e., dark or recombination current) and a lower interface photovoltage via the same fundamental mechanism as described in the previous paragraph. The potential of oxidizing the surface states is known to be at ~1.40−1.45 V vs RHE, based on capacitance measurements on similar samples.[40] The decrease in photovoltage starts when V_{cat} is ~1.45 V vs RHE; the similarity in potential is evidence in support of the idea that the surface states contribute to the reduced photovoltage.

Photogenerated Hole Transport at the SemlCat Interface. The fate of photogenerated holes on the surface of α-Fe_2O_3 coated with catalysts like Co-Pi and Ni(Fe)OOH is important and has invoked much discussion.[7,14,15,17,41] As highlighted in the introduction, transient absorption studies have suggested that increased lifetime of holes on the surface of α-Fe_2O_3 is possible with large applied anodic biases.[14] A comparable concentration of putative long-lived photogenerated holes were also seen on the CoO_x and Ga_2O_3-decorated α-Fe_2O_3 surfaces with cathodic shifts in the photocurrent onset potential, which was attributed to increased band bending of α-Fe_2O_3 with such surface decoration.[14,15] Additionally, IMPS data was used to argue that α-Fe_2O_3 decorated with $NiFeO_x$ has a lower rate of surface hole transfer.[17] These results have been used to support the view that the electrocatalyst enhances OER primarily by inducing favorable band bending in α-Fe_2O_3 or passivating surfaces instead of by harvesting holes and driving catalysis.[15] Recent related work using photoinduced absorption measurements on $BiVO_4$ have further suggested that holes are not effectively collected by the catalyst relative to direct water oxidation pathways on the semiconductor surface.[42] PEIS and

DOI: 10.1021/acscentsci.7b00310
ACS Cent. Sci. 2017, 3, 1015−1025

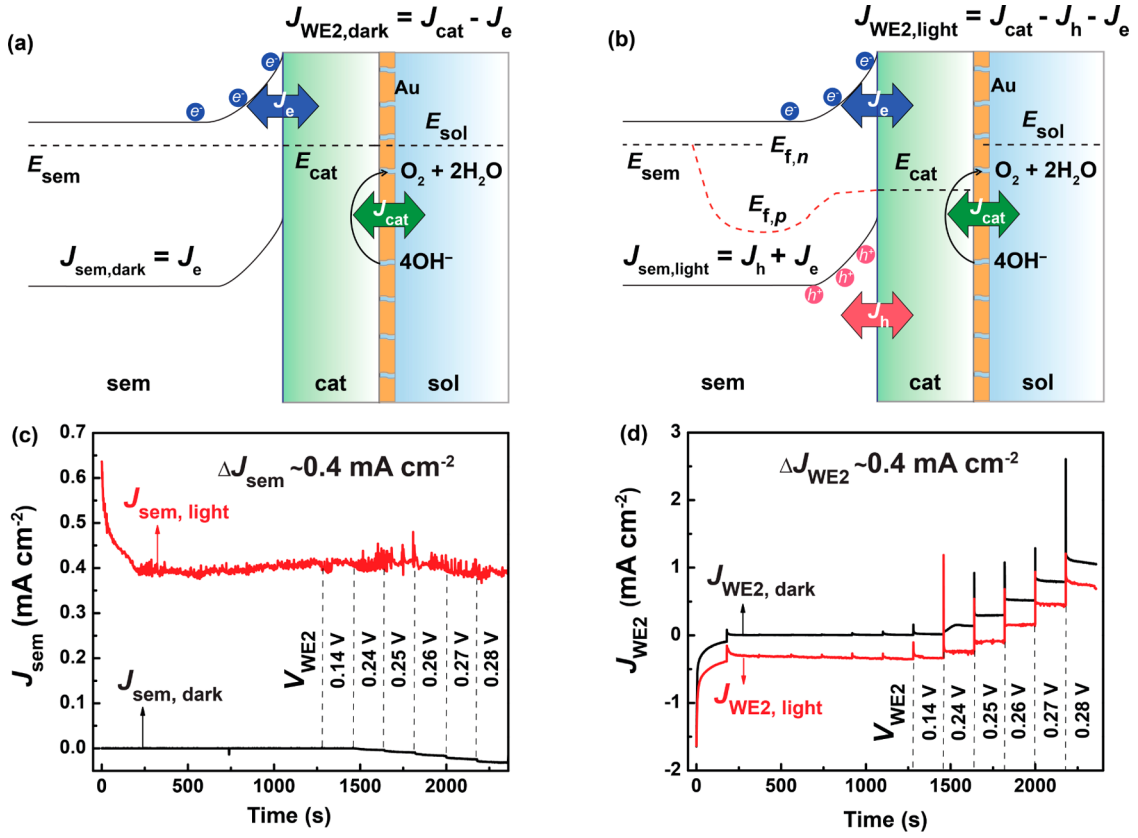

Figure 4. Photogenerated hole transfer at the interface of α-Fe_2O_3|$Ni_{0.8}Fe_{0.2}O_x$. (a) Band bending schematic of the interface in the dark. (b) Band bending schematic of the interface under illumination. (c) Current densities of α-Fe_2O_3 when WE1 is held at 0 V vs ε_{o_2/OH^-} both in the dark (black curve) and under illumination (red curve) while controlling the potentials of the catalyst in a chronoamperometry experiment. (d) Current densities measured from WE2 under different V_{cat} vs ε_{o_2/OH^-} with V_{sem} held at 0 V vs ε_{o_2/OH^-} in the dark (black curve) and under illumination (red curve). Because WE2 holds the potential of the catalyst at fixed values, any photoexcited holes injected from the semiconductor must be collected at WE2—otherwise the catalyst potential would change.

photoelectrochemical analysis from Hamann, however, suggests that electrocatalysts, such as Co-Pi and NiOOH, indeed collect holes from α-Fe_2O_3.[7,10]

The in situ potential measurement reported here for the Ni(Fe)OOH film on α-Fe_2O_3 shows that V_{WE2} (V_{cat}) abruptly increases near the photocurrent onset (Figure 3c), which is direct proof of positive charge accumulation in the electrocatalyst layer in accord with prior PEIS results. Since the dark measurements show very slow catalyst charging, which only occurs at very anodic applied V_{sem}, the source of the positive charge in an illuminated device must be photogenerated hole injection from the semiconductor to the electrocatalyst. The magnitude of the potential build-up in the catalyst layer by the hole injection from hematite (0.25 V vs ε_{o_2/OH^-}) is sufficient to drive the water oxidation reaction. This is confirmed by the steady-state current density of $Ni_{0.8}Fe_{0.2}O_x$ measured from WE2, which shows the catalyst can drive ~0.4 mA·cm^{-2} catalytic current at this potential in the dark (Figure S8). Additionally, as shown in the inset of Figure 3b, the catalyst layer is charged to identical potentials driving OER for a given current density independent of whether the holes originate from ITO or are photogenerated in hematite. These data suggest strongly that the $Ni_{0.8}Fe_{0.2}O_x$ films deposited in this way operate identically as catalytic layers both on ITO and hematite. Nonetheless, such potential measurements are unable to quantify the fraction of holes collected by the electrocatalyst layer as a function of potential.

Quantitative current density measurements through both WEs (J_{sem} and J_{WE2}) were performed with the α-Fe_2O_3|$Ni_{0.8}Fe_{0.2}O_x$|Au DWE to directly track the path of the photogenerated holes on the surface α-Fe_2O_3. The potential-dependent currents measured at the semiconductor back contact in the dark and under illumination can be decomposed into electron (J_e) and hole (J_h) currents as follows (assuming current continuity and unity transfer for both electrons and holes from the semiconductor to catalyst).

$$\text{Dark: } J_{sem,dark} = J_e$$
$$J_{WE2,dark} = J_{cat} - J_{sem,dark} = J_{cat} - J_e \quad (4)$$

$$\text{Illuminated: } J_{sem,light} = J_e + J_h$$
$$J_{WE2,light} = J_{cat} - J_{sem,light} = J_{cat} - J_e - J_h \quad (5)$$

Notice the difference between dark and illuminated currents for both J_{WE1} (J_{sem}) and J_{WE2} are equal in magnitude to J_h, if hole transfer is 100% efficient.

The potential of α-Fe_2O_3 (V_{sem}) was held at 0 V vs ε_{o_2/OH^-}, while V_{WE2} was controlled from WE2. The currents at each contact were recorded simultaneously via WE1 and WE2.

DOI: 10.1021/acscentsci.7b00310
ACS Cent. Sci. 2017, 3, 1015−1025

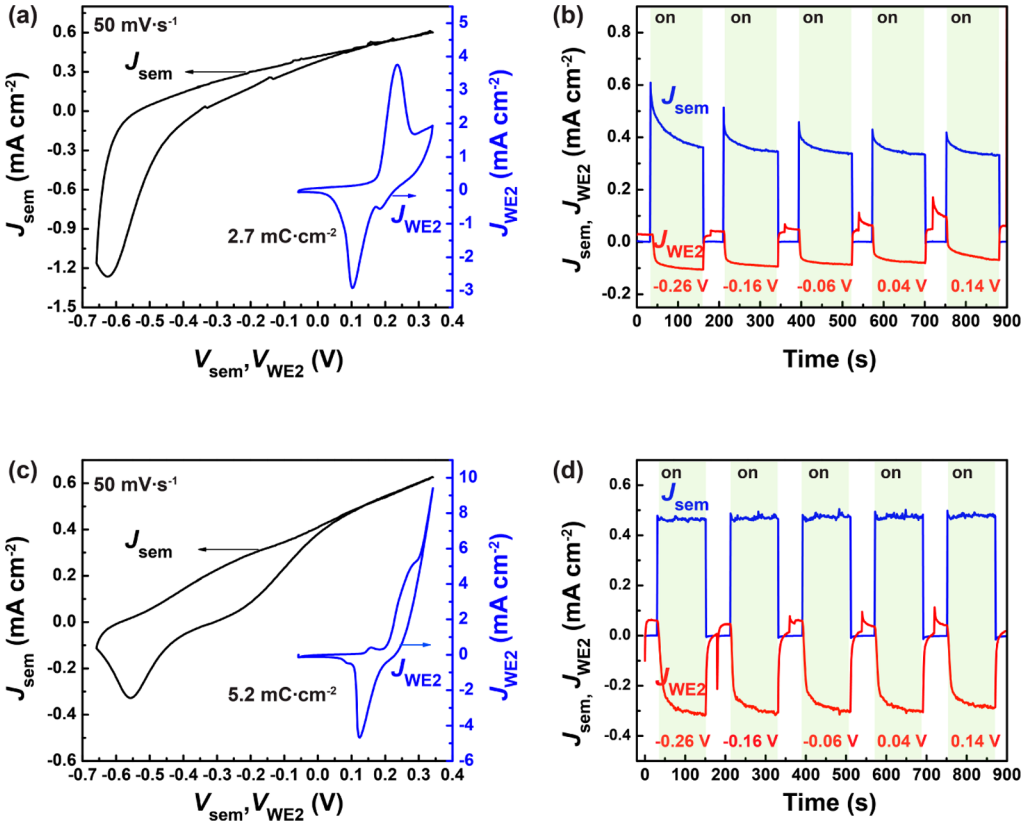

Figure 5. Photogenerated hole transfer at the interface of partially activated α-Fe_2O_3|$Ni_{0.8}Fe_{0.2}O_x$ electrodes. (a) Illuminated CVs for a representative "partially activated" DWE device under illumination measured through WE1 and WE2 separately. (b) In situ measurements of J_{WE2} and J_{sem} with V_{sem} = 0 V vs ε_{o_2/OH^-} and V_{WE2} held at potentials from −0.26 to 0.26 V vs ε_{o_2/OH^-} in chronoamperometry steps under chopped illumination show 35% efficiency of photohole collection through WE2. (c) Illuminated CVs for a representative "more-activated" DWE device under illumination measured through WE1 and WE2 separately. (d) In situ measurements of J_{WE2} and J_{sem} with V_{sem} = 0 V vs ε_{o_2/OH^-} and V_{WE2} held at potentials from −0.26 to 0.26 V vs ε_{o_2/OH^-} in chronoamperometry steps under chopped illumination show 67% efficiency of photohole collection through WE2.

Figure 4 demonstrates the collection of photogenerated holes from the hematite in the catalyst layer. When illuminated, the steady-state J_{sem} is ∼0.4 mA cm^{-2} at V_{sem} = 0 V vs ε_{o_2/OH^-} (Figure 4c)—this is the anodic photocurrent generated by the hematite, and there is little electron transfer at this V_{sem} as evident from the lack of dark current at the same voltage. To test whether photogenerated holes transfer into the catalyst layer or go directly into the solution, we measure J_{WE2} as a function of V_{WE2} = V_{cat} under both light and dark conditions (Figure 4d). In the dark, J_{WE2} increases when V_{cat} is increased by applying a potential to WE2 above 0.24 V vs ε_{o_2/OH^-}, consistent with the onset of (dark) water oxidation current. Similar behavior is observed under illumination, except that J_{WE2} decreased for all V_{cat} by ∼0.4 $mAcm^{-2}$—a current density roughly equal and opposite to the hole photocurrent density measured at WE1.

Because WE2 holds V_{cat} at a fixed value, any holes injected from the semiconductor must be removed through WE2 by the potentiostat to maintain that constant potential (assuming the catalyst is sufficiently conductive to prevent a substantial potential gradient across the catalyst). It is for this reason the current measured at WE2 decreases by the same magnitude as the photocurrent. Therefore, the data in Figure 4c,d show that holes are collected by the catalyst layer and do not substantially drive water oxidation on the hematite surface directly under these conditions (other conditions are discussed in more detail below). Furthermore, hole collection by the catalyst layer persists, even when the catalyst is biased into the OER regime ($V_{cat} \geq$ 0.24 V vs ε_{o_2/OH^-}). For example, Figure 4d shows that when the catalyst is biased at 0.28 V vs ε_{o_2/OH^-} and passing ∼1 mA·cm^{-2} of OER current in the dark, photoinjected holes are still collected by the catalyst with similar efficiency.

In addition to the direct measurements of photogenerated hole transfer across the semlcat interface with the DWE technique, we collected transient photocurrent and photoelectrochemical impedance spectroscopy data from both catalyzed and bare hematite electrodes for comparison. As shown in Figure S9, and consistent with previous reports,[10] the decay of photocurrent for $Ni_{0.8}Fe_{0.2}O_x$ catalyzed α-Fe_2O_3 is slower compared to the bare Fe_2O_3 electrode. The larger anodic and cathodic peaks of the catalyzed electrode further indicate charge transfer between the semiconductor and catalyst. Analysis of the PEIS data based on the equivalent circuit proposed previously[7] is also consistent with catalyst charging (Figure S10). However, neither of these traditional techniques report on the catalyst potential *in operando*, nor do they allow for quantifying the hole injection efficiency into the catalyst or determine what fraction of the holes drive OER on the catalyst versus on the semiconductor surface. Because hole transfer efficiencies cannot be measured by impedance or photocurrent transients, we cannot directly compare the data to the DWE data. The DWE technique is therefore a

DOI: 10.1021/acscentsci.7b00310
ACS Cent. Sci. 2017, 3, 1015−1025

complementary, but more direct, measurement of the interface properties relative to PEIS and transient photocurrent measurements.

Role of Electrocatalyst Film Activation. The physical and electrochemical properties of the catalyst layer are important for photogenerated hole collection. Young et al. showed that the activation of ALD-deposited NiO_x layer to electrolyte-permeable hydroxide/oxyhydroxide improves the photoelectrochemical performance of hematite.[10] In cases where the electrocatalyst film is not entirely activated, i.e., not completely converted to the electrolyte-permeable oxyhydroxide phases or not electrochemically accessible (as determined by the number of Ni sites from the reduction peak integration), a smaller percentage of the photogenerated holes were collected from the electrocatalyst via WE2 (Figure 5). According to eqs 4 and 5, $\Delta J_{sem} = J_{sem,light} - J_{sem,dark}$ reflects the photoinduced hole current at the semiconductor surface and $\Delta J_{WE2} = J_{WE2,dark} - J_{WE2,light}$ reflects the holes extracted by WE2 under illumination that have been injected from the semiconductor into the catalyst.

The illumination was chopped to record the current density changes of both WEs and thus the hole transfer from the semiconductor to the electrocatalyst layer under different $V_{WE2} = V_{cat}$ (Figure 5b,d). The appearance of photocurrent in J_{sem} leads to the decrease of J_{WE2}, for the reasons described above. The ratio $\Delta J_{WE2}/\Delta J_{sem}$ was then used to determine the apparent hole transfer efficiency. The data in Figure 5 suggest that the hole transfer efficiency is related to the percentage of electrochemically active Ni sites. A catalyst film with 1.7×10^{16} cm^{-2} (2.7 $mC \cdot cm^{-2}$) Ni sites redox activated (Figure 5a) collects only 35% of the photogenerated holes through WE2 (Figure 5b), while a film with 3.2×10^{16} cm^{-2} (5.2 $mC \cdot cm^{-2}$) Ni sites redox activated (Figure 5c) increases the efficiency to 67% (Figure 5d). A portion of the catalyst layer may not be sufficiently electrically "wired" to the Au WE2, and thus holes from those regions cannot be collected. Photogenerated holes in these regions of the film then must accumulate and drive OER either through surface Fe(IV)-oxo groups, as has been observed on bare electrodes,[40] or via catalyst regions isolated from the WE2 but in contact with the hematite surface. The small redox peaks more cathodic to the major ones in Figure 5c could be an indication of the local heterogeneity of the catalyst film. We have measured a variety of other DWE electrode devices and found that the apparent hole transfer efficiency measured at WE2 can vary between 35−95%, depending on the portion of the activated catalyst film and the integrity of the top Au contact.

The results on the partially activated samples may be important in the context of the various differing proposals on the role of the catalyst layer. The chemical state of the catalyst film significantly affects its ability to drive the water oxidation reaction.[33] Catalysts deposited in ways that lead to electronic insulators cannot participate in water oxidation, and thus those regions of any catalyst films will appear inactive by in situ measurements. Fully activated films appear to nearly quantitatively collect holes from hematite, even after fully oxidizing the catalyst such that it is driving substantial OER current, and its potential is far positive of ε_{o_2/OH^-}. Our observations of incomplete hole collection at the Au WE2 in the case of the partially activated films is thus likely because the catalyst and/or interface is heterogeneous. Similarly, for electrodeposited catalyst films studied by other techniques,[42] heterogeneity of the film morphology, contact to the semiconductor surface, or electrical integration with the remainder of the catalyst film could all affect the ability to observe quantitative hole collection by the catalyst by optical or electrical techniques regardless of the underlying charge transfer processes.

Barroso et al. showed that TSA studies provide no evidence of hole transfer to the cobalt-based layer under different applied biases.[14] With anodic biasing of the semiconductor, the decreased electron/hole recombination was proposed to generate long-lived holes at the semiconductor surface,[14] which make direct water oxidation more favorable. We changed the band bending in α-Fe_2O_3 by increasing V_{sem} by 0.1 V (to 0.1 V vs ε_{o_2/OH^-}), and the photocurrent density increased from 0.40 to 0.48 $mA \cdot cm^{-2}$ (Figure S11). This is likely due to higher efficiency of electron and hole separation in hematite.[37] With a higher density of hole flux on the α-Fe_2O_3 surface, the charge-transfer efficiency from the semiconductor to the electrocatalyst is ∼90% with $V_{WE2} \leq 0.25$ V vs ε_{o_2/OH^-} and ∼60% when V_{WE2} biased to 0.28 V vs ε_{o_2/OH^-} (Figure S11) for this catalyst film (the same device as shown in Figure 4). Additional data supporting the findings of hole transfer to the catalyst layer under a wide variety of biasing conditions for WE1 and WE2 are shown in Figure S12. The decrease in hole transfer efficiency at very oxidizing V_{cat} and $V_{sem} = 0.1$ V may be because the OER becomes sufficiently fast that the holes are consumed before they can be measured by the Au WE2 contact (i.e., the catalyst is not sufficiently conductive to prevent the photoinjected holes from causing a potential gradient across the film that changes the catalyst OER rate in the dark versus the light, leading to a breakdown of the assumptions described above).

The sum of these results demonstrates that the kinetics of hole transfer to the electrocatalyst from the semiconductor generally outcompetes that of direct water oxidation on the electrode surface, even when there is a significant driving force for direct water oxidation processes and/or when the catalyst is highly oxidized. Such results are consistent with the view of the oxidized Ni(Fe)OOH catalyst having a delocalized band structure (i.e., such as that found from DFT calculations[43,44]) that should be able to collect holes effectively over a large range of energies.

CONCLUSION

The deposition of $Ni_{0.8}Fe_{0.2}O_x$ films onto hematite induces a cathodic shift in the water oxidation photocurrent onset potential, increasing photoelectrode efficiency. $Ni_{0.8}Fe_{0.2}O_x$ thin films are a model electrocatalyst known to have exceptional OER activity. DWE (photo)electrochemical techniques provide new insight into the intrinsic properties of $Ni_{0.8}Fe_{0.2}O_x$ films and of the α-Fe_2O_3|$Ni_{0.8}Fe_{0.2}O_x$ interface. The electrical conductivity of the electrolyte-permeable $Ni_{0.8}Fe_{0.2}O_x$ catalyst depends sensitively on the applied potential and hence nominal oxidation state of the Ni cations in the film. The catalyst film is an electrical insulator in the resting state, but becomes electrically conductive after oxidation to the active catalyst state. This oxidation of $Ni_{0.8}Fe_{0.2}O_x$ also affects the α-Fe_2O_3|$Ni_{0.8}Fe_{0.2}O_x$ interface, as evidenced by the decreased sem|cat photovoltage when the catalyst is driven to highly oxidizing potentials. The oxidized, electrically conducting catalyst film effectively collects photoexcited holes from the semiconductor surface. This hole transfer efficiency is not substantially affected by the oxidation level of the catalyst or by the driving force for

DOI: 10.1021/acscentsci.7b00310
ACS Cent. Sci. 2017, 3, 1015−1025

water oxidation directly at the α-Fe_2O_3 surface (controlled by the applied V_{sem}) over a large range, consistent with fast kinetics for hole injection into the electrically conducting catalyst layer. Heterogeneity in the catalyst properties, for example, the extent of electrochemical activation, however, appear to lead to differences in the average hole transfer efficiency which could explain possible differences with some previous work.

Here we have demonstrated the applicability of the DWE technique to a low band gap polycrystalline (i.e., more practical) photoelectrode. This advance suggests the DWE technique is broadly applicable to thin film photoelectrode materials, including both photoanodes and photocathodes. Further study of catalysts with different Fermi levels, electronic structure, and/or redox behaviors would be useful to tune the interface and design more-effective photoanode systems for PEC water splitting. Specifically, a systematic study of tuning the Ni/Fe ratio in the Ni(Fe)O_x electrocatalyst would be interesting as the Fe content effects the potential of the Ni redox waves. Additionally, the density of surface states on the hematite semiconductor is known to play a role in interface photovoltage build-up and charge extraction,[28] and merits further investigation in the context of the semlcat systems. Insight into the heterogeneity of the interface photovoltage generation and charge-transfer processes would also be useful and may be possible by applying techniques with nanoscale spatial resolution, for example, electrochemical atomic force microscopy.[45]

■ ASSOCIATED CONTENT

Supporting Information

The Supporting Information is available free of charge on the ACS Publications website at DOI: 10.1021/acscentsci.7b00310.

Sample preparation, materials characterization, additional schemes and data figures (PDF)

■ AUTHOR INFORMATION

Corresponding Author

*E-mail: swb@uoregon.edu.

ORCID

Thomas W. Hamann: 0000-0001-6917-7494

Shannon W. Boettcher: 0000-0001-8971-9123

Notes

The authors declare no competing financial interest.

■ ACKNOWLEDGMENTS

This work was primarily funded by the Department of Energy, Basic Energy Sciences, Award Number DE-SC0014279. S.W.B. also acknowledges support from the Sloan and Dreyfus foundations. H.H. and T.W.H. were responsible for growing the hematite photoelectrodes by ALD supported by NSF Award CHE-1664823 and provided insightful comments regarding the data analysis. We also thank Professor Mark Lonergan and Dr. Fuding Lin for insightful scientific discussions.

■ REFERENCES

(1) Khaselev, O.; Turner, J. A. A monolithic photovoltaic-photoelectrochemical device for hydrogen production *via* water splitting. *Science* **1998**, *280*, 425−427.

(2) Lewis, N. S. Introduction: solar energy conversion. *Chem. Rev.* **2015**, *115*, 12631−12632.

(3) Mayer, M. T.; Du, C.; Wang, D. W. Hematite/Si nanowire dual-absorber system for photoelectrochemical water splitting at low applied potentials. *J. Am. Chem. Soc.* **2012**, *134*, 12406−12409.

(4) Peter, L. M.; Wijayantha, K. G. U. Photoelectrochemical water splitting at semiconductor electrodes: fundamental problems and new perspectives. *ChemPhysChem* **2014**, *15*, 1983−1995.

(5) Badia-Bou, L.; Mas-Marza, E.; Rodenas, P.; Barea, E. M.; Fabregat-Santiago, F.; Gimenez, S.; Peris, E.; Bisquert, J. Water oxidation at hematite photoelectrodes with an iridium-based catalyst. *J. Phys. Chem. C* **2013**, *117*, 3826−3833.

(6) Tilley, S. D.; Cornuz, M.; Sivula, K.; Gratzel, M. Light-induced water splitting with hematite: improved nanostructure and iridium oxide catalysis. *Angew. Chem., Int. Ed.* **2010**, *49*, 6405−6408.

(7) Klahr, B.; Gimenez, S.; Fabregat-Santiago, F.; Bisquert, J.; Hamann, T. W. Photoelectrochemical and impedance spectroscopic investigation of water oxidation with "Co-Pi"-coated hematite electrodes. *J. Am. Chem. Soc.* **2012**, *134*, 16693−16700.

(8) Kanan, M. W.; Nocera, D. G. *In situ* formation of an oxygen-evolving catalyst in neutral water containing phosphate and Co^{2+}. *Science* **2008**, *321*, 1072−1075.

(9) Du, C.; Yang, X. G.; Mayer, M. T.; Hoyt, H.; Xie, J.; McMahon, G.; Bischoping, G.; Wang, D. W. Hematite-based water splitting with low turn-on voltages. *Angew. Chem., Int. Ed.* **2013**, *52*, 12692−12695.

(10) Young, K. M. H.; Hamann, T. W. Enhanced photocatalytic water oxidation efficiency with $Ni(OH)_2$ catalysts deposited on α-Fe_2O_3 *via* ALD. *Chem. Commun.* **2014**, *50*, 8727−8730.

(11) Laskowski, F. A. L.; Nellist, M. R.; Venkatkarthick, R.; Boettcher, S. W. Junction behavior of n-Si photoanodes protected by thin Ni elucidated from dual working electrode photoelectrochemistry. *Energy Environ. Sci.* **2017**, *10*, 570−579.

(12) Kim, T. W.; Choi, K. S. Nanoporous $BiVO_4$ photoanodes with dual-layer oxygen evolution catalysts for solar water splitting. *Science* **2014**, *343*, 990−994.

(13) Zhong, D. K.; Gamelin, D. R. Photoelectrochemical water oxidation by cobalt catalyst ("Co-Pi")/α-Fe_2O_3 composite photoanodes: *o*xygen evolution and resolution of a kinetic bottleneck. *J. Am. Chem. Soc.* **2010**, *132*, 4202−4207.

(14) Barroso, M.; Mesa, C. A.; Pendlebury, S. R.; Cowan, A. J.; Hisatomi, T.; Sivula, K.; Gratzel, M.; Klug, D. R.; Durrant, J. R. Dynamics of photogenerated holes in surface modified α-Fe_2O_3 photoanodes for solar water splitting. *Proc. Natl. Acad. Sci. U. S. A.* **2012**, *109*, 15640−15645.

(15) Barroso, M.; Cowan, A. J.; Pendlebury, S. R.; Gratzel, M.; Klug, D. R.; Durrant, J. R. The role of cobalt phosphate in enhancing the photocatalytic activity of α-Fe_2O_3 toward water oxidation. *J. Am. Chem. Soc.* **2011**, *133*, 14868−14871.

(16) Huang, Z. Q.; Lin, Y. J.; Xiang, X.; Rodriguez-Cordoba, W.; McDonald, K. J.; Hagen, K. S.; Choi, K. S.; Brunschwig, B. S.; Musaev, D. G.; Hill, C. L.; Wang, D.; Lian, T. *In situ* probe of photocarrier dynamics in water-splitting hematite (α-Fe_2O_3) electrodes. *Energy Environ. Sci.* **2012**, *5*, 8923−8926.

(17) Thorne, J. E.; Jang, J. W.; Liu, E. Y.; Wang, D. W. Understanding the origin of photoelectrode performance enhancement by probing surface kinetics. *Chem. Sci.* **2016**, *7*, 3347−3354.

(18) Ponomarev, E. A.; Peter, L. M. A generalized theory of intensity-modulated photocurrent spectroscopy (IMPS). *J. Electroanal. Chem.* **1995**, *396*, 219−226.

(19) Nellist, M. R.; Laskowski, F. A. L.; Lin, F. D.; Mills, T. J.; Boettcher, S. W. Semiconductor-electrocatalyst interfaces: theory, experiment, and applications in photoelectrochemical water splitting. *Acc. Chem. Res.* **2016**, *49*, 733−740.

(20) Klaus, S.; Cai, Y.; Louie, M. W.; Trotochaud, L.; Bell, A. T. Effects of Fe electrolyte impurities on $Ni(OH)_2$/NiOOH structure and oxygen evolution activity. *J. Phys. Chem. C* **2015**, *119*, 7243−7254.

(21) Trotochaud, L.; Young, S. L.; Ranney, J. K.; Boettcher, S. W. Nickel-iron oxyhydroxide oxygen-evolution electrocatalysts: the role of intentional and incidental iron incorporation. *J. Am. Chem. Soc.* **2014**, *136*, 6744−6753.

(22) Smith, R. D. L.; Prevot, M. S.; Fagan, R. D.; Trudel, S.; Berlinguette, C. P. Water oxidation catalysis: electrocatalytic response to metal stoichiometry in amorphous metal oxide films containing iron, cobalt, and nickel. *J. Am. Chem. Soc.* **2013**, *135*, 11580−11586.
(23) Friebel, D.; Louie, M. W.; Bajdich, M.; Sanwald, K. E.; Cai, Y.; Wise, A. M.; Cheng, M. J.; Sokaras, D.; Weng, T. C.; Alonso-Mori, R.; Davis, R. C.; Bargar, J. R.; Nørskov, J. K.; Nilsson, A.; Bell, A. T. Identification of highly active Fe sites in (Ni,Fe)OOH for electrocatalytic water splitting. *J. Am. Chem. Soc.* **2015**, *137*, 1305−1313.
(24) Carroll, G. M.; Zhong, D. K.; Gamelin, D. R. Mechanistic insights into solar water oxidation by cobalt-phosphate-modified α-Fe_2O_3 photoanodes. *Energy Environ. Sci.* **2015**, *8*, 577−584.
(25) Trotochaud, L.; Mills, T. J.; Boettcher, S. W. An optocatalytic model for semiconductor-catalyst water-splitting photoelectrodes based on *in situ* optical measurements on operational catalysts. *J. Phys. Chem. Lett.* **2013**, *4*, 931−935.
(26) Lin, F. D.; Boettcher, S. W. Adaptive semiconductor/electrocatalyst junctions in water-splitting photoanodes. *Nat. Mater.* **2013**, *13*, 81−86.
(27) Mills, T. J.; Lin, F. D.; Boettcher, S. W. Theory and simulations of electrocatalyst-coated semiconductor electrodes for solar water splitting. *Phys. Rev. Lett.* **2014**, *112*, 148304.
(28) Zandi, O.; Hamann, T. W. Enhanced water splitting efficiency through selective surface state removal. *J. Phys. Chem. Lett.* **2014**, *5*, 1522−1526.
(29) Sivula, K.; Le Formal, F.; Gratzel, M. Solar water splitting: progress using hematite (α-Fe_2O_3) photoelectrodes. *ChemSusChem* **2011**, *4*, 432−449.
(30) Smith, W. A.; Sharp, I. D.; Strandwitz, N. C.; Bisquert, J. Interfacial band-edge energetics for solar fuels production. *Energy Environ. Sci.* **2015**, *8*, 2851−2862.
(31) Klahr, B.; Gimenez, S.; Fabregat-Santiago, F.; Hamann, T.; Bisquert, J. Water oxidation at hematite photoelectrodes: the role of surface states. *J. Am. Chem. Soc.* **2012**, *134*, 4294−4302.
(32) Smith, R. D. L.; Prevot, M. S.; Fagan, R. D.; Zhang, Z. P.; Sedach, P. A.; Siu, M. K. J.; Trudel, S.; Berlinguette, C. P. Photochemical route for accessing amorphous metal oxide materials for water oxidation catalysis. *Science* **2013**, *340*, 60−63.
(33) Trzesniewski, B. J.; Diaz-Morales, O.; Vermaas, D. A.; Longo, A.; Bras, W.; Koper, M. T. M.; Smith, W. A. *In situ* observation of active oxygen species in Fe-containing Ni-based oxygen evolution catalysts: the effect of pH on electrochemical activity. *J. Am. Chem. Soc.* **2015**, *137*, 15112−15121.
(34) Stevens, M. B.; Enman, L. J.; Batchellor, A. S.; Cosby, M. R.; Vise, A. E.; Trang, C. D. M.; Boettcher, S. W. Measurement techniques for the study of thin film heterogeneous water oxidation electrocatalysts. *Chem. Mater.* **2017**, *29*, 120−140.
(35) Natan, M. J.; Belanger, D.; Carpenter, M. K.; Wrighton, M. S. pH-sensitive $Ni(OH)_2$-based microelectrochemical transistors. *J. Phys. Chem.* **1987**, *91*, 1834−1842.
(36) Jang, J. W.; Du, C.; Ye, Y. F.; Lin, Y. J.; Yao, X. H.; Thorne, J.; Liu, E.; McMahon, G.; Zhu, J. F.; Javey, A.; Guo, J.; Wang, D. W. Enabling unassisted solar water splitting by iron oxide and silicon. *Nat. Commun.* **2015**, *6*, 7447.
(37) Klahr, B. M.; Hamann, T. W. Voltage dependent photocurrent of thin film hematite electrodes. *Appl. Phys. Lett.* **2011**, *99*, No. 063508.
(38) Lewis, N. S. Chemical control of charge transfer and recombination at semiconductor photoelectrode surfaces. *Inorg. Chem.* **2005**, *44*, 6900−6911.
(39) Le Formal, F.; Sivula, K.; Gratzel, M. The transient photocurrent and photovoltage behavior of a hematite photoanode under working conditions and the influence of surface treatments. *J. Phys. Chem. C* **2012**, *116*, 26707−26720.
(40) Zandi, O.; Hamann, T. W. Determination of photoelectrochemical water oxidation intermediates on haematite electrode surfaces using operando infrared spectroscopy. *Nat. Chem.* **2016**, *8*, 778−783.
(41) Gamelin, D. R. Water splitting catalyst or spectator? *Nat. Chem.* **2012**, *4*, 965−967.
(42) Ma, Y. M.; Kafizas, A.; Pendlebury, S. R.; Le Formal, F.; Durrant, J. R. Photoinduced absorption spectroscopy of CoPi on $BiVO_4$: the function of CoPi during water oxidation. *Adv. Funct. Mater.* **2016**, *26*, 4951−4960.
(43) Tkalych, A. J.; Yu, K.; Carter, E. A. Structural and electronic features of β-$Ni(OH)_2$ and β-NiOOH from first principles. *J. Phys. Chem. C* **2015**, *119*, 24315−24322.
(44) Fidelsky, V.; Butera, V.; Zaffran, J.; Toroker, M. C. Three fundamental questions on one of our best water oxidation catalysts: a critical perspective. *Theor. Chem. Acc.* **2016**, *135*, 162.
(45) Nellist, M. R.; Chen, Y.; Mark, A.; Gödrich, S.; Stelling, C.; Jiang, J.; Poddar, R.; Li, C.; Kumar, R.; Papastavrou, G.; Retsch, M.; Brunschwig, B. S.; Huang, Z.; Xiang, C.; Boettcher, S. W. Atomic force microscopy with nanoelectrode tips for high resolution electrochemical, nanoadhesion and nanoelectrical imaging. *Nanotechnology* **2017**, *28*, 095711.

DOI: 10.1021/acscentsci.7b00310
ACS Cent. Sci. 2017, 3, 1015−1025